Progress In Electromagnetics Research B, Vol. 13, 133–150, 2009

A DIELECTRIC RESONATOR-BASED ROUTE TO LEFT-HANDED METAMATERIALS

J. Wang, S. Qu, H. Ma, J. Hu, Y. Yang, and X. Wu

Air Force Engineering University
Xi'an, Shaanxi 710051, China

Z. Xu

Electronic Materials Research Laboratory
Key Laboratory of the Ministry of Education
Xi'an Jiaotong University
Xi'an, Shaanxi 710049, China

M. Hao

Northwest University
Xi'an, Shaanxi 710127, China

Abstract—In this paper, a new route for the realization of left-handed metamaterials (LHMs) is suggested. It is based on commercially available dielectric resonators with low loss and high temperature stability. By etching simple metallic strips on surface of dielectric resonators, the desired resonance modes can be enhanced while the undesired suppressed. In this way, resonance frequency of desired resonance modes can be tuned to the frequency range of interest. As a typical example, a wide-angle polarization-independent planar LHM based on disk-like dielectric resonators is proposed. Negative permeability and permittivity are realized by etching metallic strips along the electric field orientations of $TE_{01\delta}$ and $HEM_{11\delta}$ modes, respectively.

Corresponding author: J. Wang (wangjiafu1981@126.com).

1. INTRODUCTION

Left-handed metamaterials (LHMs) with simultaneously negative permeability and permittivity have been attracting great attentions since the initiatory work of Pendry and Smith [1, 2]. Because of their great potential applications in many fields, the development of new kinds of LHMs has gained great impetus. A great variety of LHMs have been designed and fabricated. Generally speaking, the existent LHMs fall into three categories. LHMs in the first category realize their negative permeability and/or permittivity by the resonances of some certain metallic patterns etched on substrates. LHM unit cells, like S-shaped [3], Ω-shaped [4], coplanar resonator unit cells [5], fall into this category. For these LHMs, the magnetic fields are required to thread through the metallic patterns in order to have a magnetically driven resonance and hence a negative effective permeability. This brings an annoying problem for these unit cells: incident waves must be in parallel with substrates, which makes them quite troublesome to be fabricated and used.

LHMs in the second category are called planar LHMs [6–12]. Unit cells of planar LHMs are usually such that identical metallic patterns are etched on both sides of substrates. They realize negative permeability by the coupling between the two identical metallic patterns and negative permittivity by the interactions between two neighboring metallic patterns on the same side of the substrates. Although planar LHMs are also realized by using metallic patterns, they are different from LHMs in the first category in that they allow the incident waves to be perpendicular to substrates, so they are much more convenient to be fabricated and used. Moreover, planar LHMs can be made in the form of bulk materials.

Recently, many researchers are focusing on all-dielectric realization of LHMs [13–19]. Many all-dielectric LHM unit cells, such as spherical [13], cubic [14] and disk-like unit cells [15], were proposed. These unit cells are based on different resonance modes in the unit cells which behave like dielectric resonators (DRs). Under a certain resonance mode, the effective permeability or/and permittivity are negative. The key to realizing all-dielectric metamaterials is to get the proper resonance modes. High-permittivity ceramics with good temperature stability and low dielectric loss are required to realize all-dielectric LHMs. However, to date, the loss tangent of most high-permittivity dielectrics is quite high and their temperature stability is not so good. In contrast, some DRs made of microwave ceramic materials, such as $Ba_2Ti_9O_{20}$, $BaTi_4O_9$, (Zr, Sn)TiO_4, mostly have low loss tangents and good temperature stability. Moreover, they have high Q

factors. It comes to us naturally that these sophisticated microwave DRs are ideal candidates for designing LHMs. However, a problem arises. The dielectric constants of most sophisticated microwave ceramic materials are between 30∼40, much less than some all-dielectric unit cells require [17, 18]. For these DRs, their resonance frequencies are usually so high that effective medium theory cannot be used to characterize them. As a result, it is desirable to tune their resonance frequencies down to lower frequencies that we are interested in.

In this paper, we proposed a new route to the realization of LHMs based on commercially available DRs with low loss and good temperature stability. By etching metallic strips on surface of DRs, resonance frequencies of desired resonance modes can be tuned down to the frequency range of interest. As an example, a planar LHM based on disk-like DRs was presented. By etching metallic strips along the electric field orientations of $TE_{01\delta}$ and $HEM_{11\delta}$ modes on two separate DRs, negative permeability and permittivity were realized, respectively. By combing the two DRs etched with metallic strips, a planar LHM unit cell was realized. Because of the good symmetry of the unit cell, the proposed planar LHM is polarization-independent. Moreover, the negative refraction index band keeps almost the same under a wide range of incident angles.

2. DESIGN

Figure 1 shows some commercially available microwave DRs. Microwave DRs are often made of high-purity, high-density ceramics to minimize loss. Traditionally, they are used to miniaturize microwave circuits. Now, there have been a variety of shapes available for custom application requirements. Of all these shapes, the disk-like DR shown

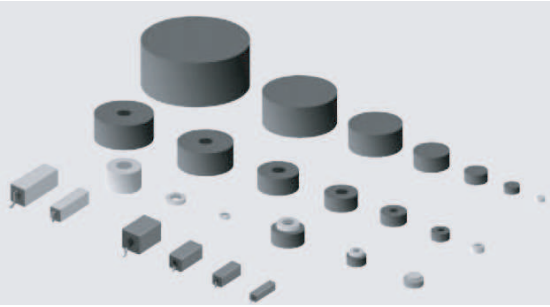

Figure 1. Some commercially available microwave dielectric resonators.

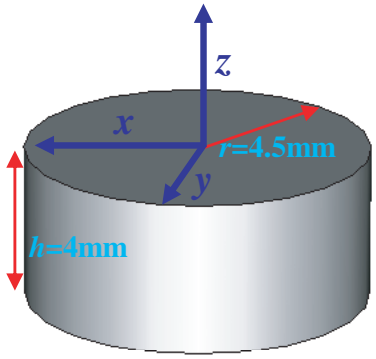

Figure 2. A disk-like microwave dielectric resonator.

in Figure 2 is the most typical. It is a TE mode resonator and is traditionally used for stabilizing frequency in microwave oscillators. In this paper, we take the disk-like DR shown in Figure 2 as a typical example to illustrate the new route for designing DR-based LHMs. The selected disk-like DRs are made of (Zr, Sn)TiO_4. The dielectric constant is $\varepsilon_r = 38$. Radius and height of the DR are $r = 4.5\,\text{mm}$ and $h = 4\,\text{mm}$, respectively. For a bare DR shown in Figure 2, the resonance frequency range is $5.87 \sim 6.38\,\text{GHz}$. In this frequency range, the wavelength λ is about 50 mm, about 5.5 times the diameter of DR. To characterize the DR using the effective medium theory, the wavelength must be more than 7 times the sizes of DRs. So, it is necessary to tune the resonance frequency range down to lower ranges.

2.1. Design of the DR-based Negative-permeability Metamaterials

The lowest resonance mode of disk-like DR is $TE_{01\delta}$ mode. Figure 3(a) shows the electric field distribution in (x, y) plane under $TE_{01\delta}$ mode. Metallic strips along the electric field orientation can change the electric field distribution in (x, y) plane [20]. Since the metallic strips form a circular ring, the electric field can drive a circular current in the circular ring. The circular current will produce strong magnetic fields threading through the metallic ring. Thus, a magnetically driven resonance and hence a negative effective permeability can be realized.

Based on the above analysis, we designed the negative-permeability unit cell based on disk-like DRs. Figure 4(a) shows the negative-permeability unit cell. On the two end surfaces, two identical copper rings are etched. The width and outer radius of the copper rings

are $w = 1.0\,\text{mm}$ and $R = 2.5\,\text{mm}$. Figure 4(b) shows the magnetic metamaterial using the negative-permeability unit cell. The distance between each two unit cells is $a = 10\,\text{mm}$.

By numerical simulations, we investigated a layer of magnetic

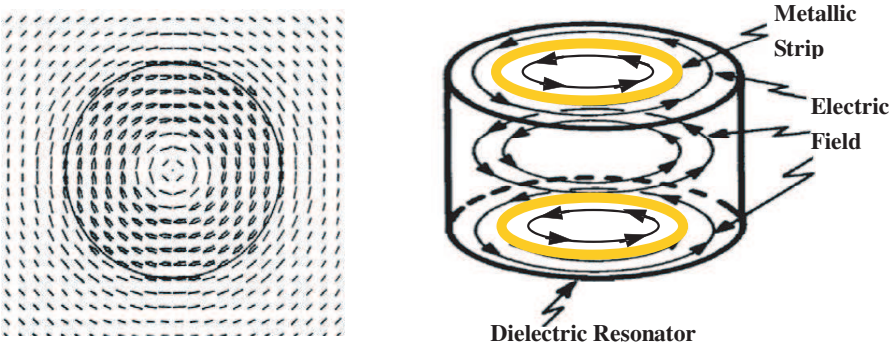

(a) (b)

Figure 3. Schematic illustration of electric field distribution in the (x, y) plane under $\text{TE}_{01\delta}$ mode (a) and method of tuning down the resonance frequency of $\text{TE}_{01\delta}$ mode by etching metallic strips along the electric field orientation.

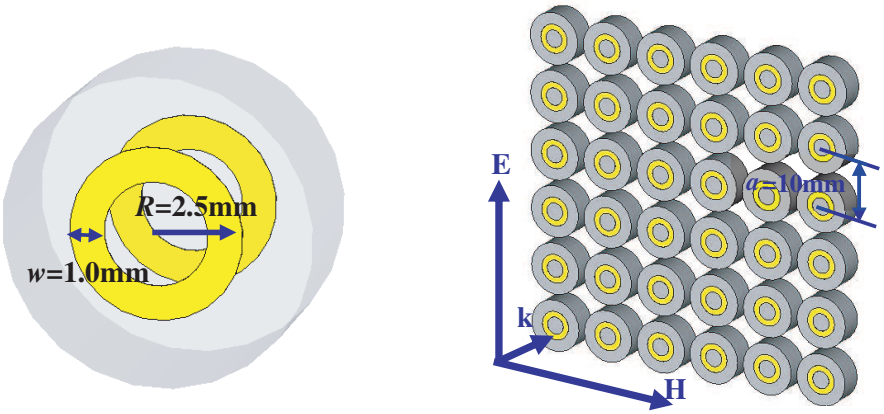

(a) (b)

Figure 4. The negative-permeability unit cell (a) and one layer of magnetic metamaterial which is one-unit-cell thick in the propagation direction and infinite in two other directions (b).

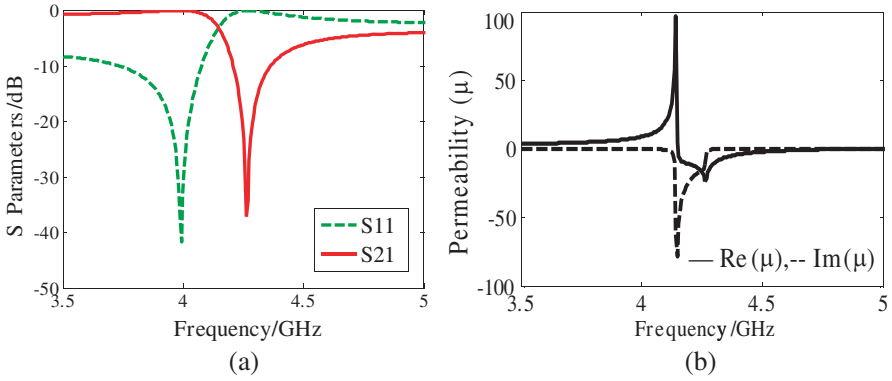

Figure 5. Transmission spectrum (a) and retrieved effective permeability (b) for the one-unit-cell thick magnetic metamaterial shown in Figure 4(b).

metamaterial which is one-unit-cell thick in the propagation direction and infinite in two other directions. Computer simulations were performed using the FDTD solver of CST Microwave Studio. Polarizations of incident waves are shown in Figure 4(b). Incident plane waves are incident normally onto the magnetic metamaterial along the z axis direction of the disk-like DRs. Periodic boundary conditions (PBCs) are imposed onto the unit cell in both x and y direction to calculate the scattering parameters in the simulations. The simulated transmission spectrum is shown in Figure 5(a). As shown in Figure 5(a), there is a stop-band around 4.25 GHz, which indicates a magnetic resonance. Effective constitutive parameters can be retrieved from scattering parameters obtained by simulations or experiments [21–23]. The retrieved effective permeability is shown in Figure 5(b). There is an obvious magnetic resonance in Figure 5(b). In the frequency range 4.15 $\sim$ 4.85 GHz, real part of the effective permeability is negative.

2.2. Design of the DR-based Negative-permittivity Metamaterials

The second lowest resonance mode of disk-like DR is $\mathrm{HEM}_{11\delta}$ mode. Figure 6(a) shows the electric field distribution in (x, z) plane under $\mathrm{HEM}_{11\delta}$ mode. To tune down the resonance frequency of $\mathrm{HEM}_{11\delta}$ mode, two metallic strips perpendicular to each other can be etched on surface of the DR, as shown in Figure 6(b). The two metallic strips form two rectangular rings. On the two circular end faces,

the two metallic strips intersect with each other at the center of the circle. In this way, the electric fields under $HEM_{11\delta}$ mode are enclosed by the rectangular metallic rings, as shown in Figure 6(b). Thus, magnetic resonance in $HEM_{11\delta}$ mode is suppressed while only the electric resonance in $HEM_{11\delta}$ mode is maintained and tuned down.

Based on the above analysis, the negative-permittivity unit cell based on disk-like DRs is designed. Figure 7(a) shows the negative-permittivity unit cell. Two identical perpendicular rectangular copper rings are etched on surface of the DR. The width of the copper rings is $w = 1.0\,\text{mm}$. Figure 7(b) shows the electric metamaterial using the negative-permittivity unit cell. The distance between each two unit cells is $a = 10\,\text{mm}$.

By numerical simulations, we investigated a layer of electric metamaterial which is one-unit-cell thick in the propagation direction and infinite in two other directions. Polarizations of incident waves are shown in Figure 7(b). Incident plane waves are incident normally onto the electric metamaterial along z direction. The simulated transmission spectrum is shown in Figure 8(a). As shown in Figure 8(a), there is a stop-band around 4.2 GHz, which indicates an electric resonance. The retrieved effective permittivity is shown in Figure 8(b). In Figure 8(b), there is an obvious electric resonance. In the frequency range $4.12 \sim 4.26\,\text{GHz}$, real part of the effective permittivity is negative.

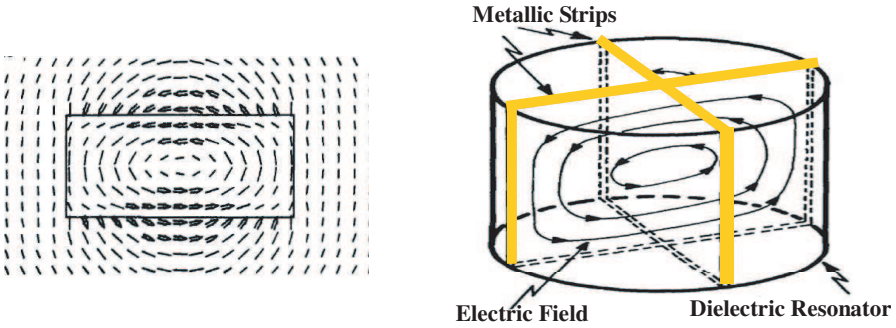

Figure 6. Electric field distribution in (x, z) plane under $HEM_{11\delta}$ mode (a) and method of tuning down the resonance frequency of $HEM_{11\delta}$ mode by etching metallic strips along the electric field orientation. The two metallic strips are perpendicular to each other.

2.3. Design of the DR-based Left-handed Metamaterials

By combining the negative-permeability and negative-permittivity unit cells, a planar LHM is expected to be realized. Figure 9(a) shows the proposed planar LHM. In the LHM, the the negative-permeability and negative-permittivity unit cells are arranged alternatively both in x and y directions. The distance between each two adjacent unit cells is 10 mm.

By numerical simulations, we investigated a layer of the LHM which is one-unit-cell thick in the propagation direction and infinite in x and y directions. Polarizations of incident plane waves are shown in Figure 9(a). Plane waves are incident normally onto the LHM. Figure 9(b) gives the magnitudes of simulated S_{11} and S_{21} parameter in dB under normally incident plane waves. As shown in Figure 9(b), there is no stop-band in the spectrum of the proposed LHM. In the frequency range where originally there is a stop-band in both the transmission spectra of the magnetic and electric metamaterials, the transmission is quite high. This newly-emerging pass-band is the very pass-band that is expected to be left-handed.

Effective constitutive parameters were retrieved from the simulated scattering parameters. Figures 10(a), (b), (c) and (d) show the retrieved effective permeability, permittivity, impedance and refraction index under normal incidence. As shown in Figures 10(a) and (b), the real part of effective permeability is negative in 4.19 $\sim$

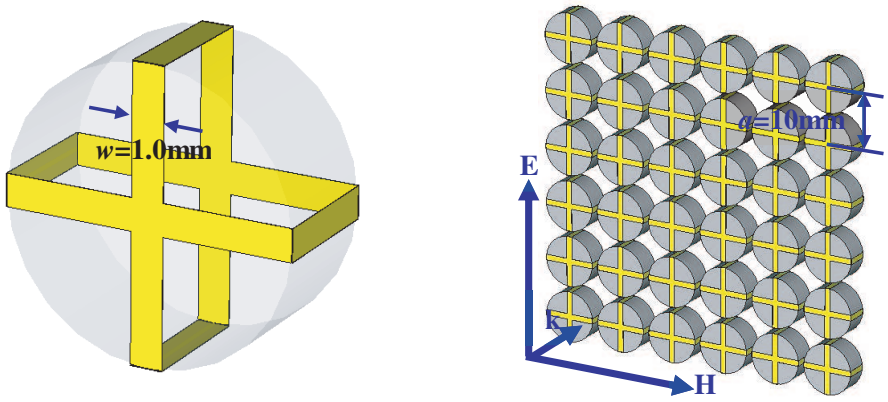

Figure 7. The negative-permittivity unit cell (a) and one layer of electric metamaterial which is one-unit-cell thick in the propagation direction and infinite in two other directions (b).

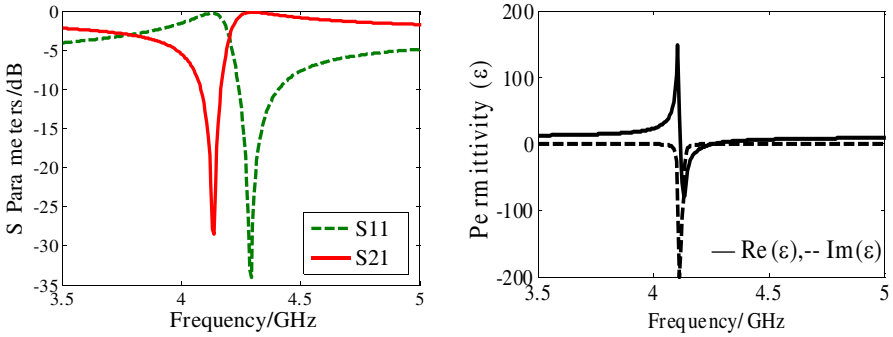

Figure 8. Transmission spectrum (a) and retrieved effective permittivity (b) for the one-unit-cell thick electric metamaterial shown in Figure 7(b).

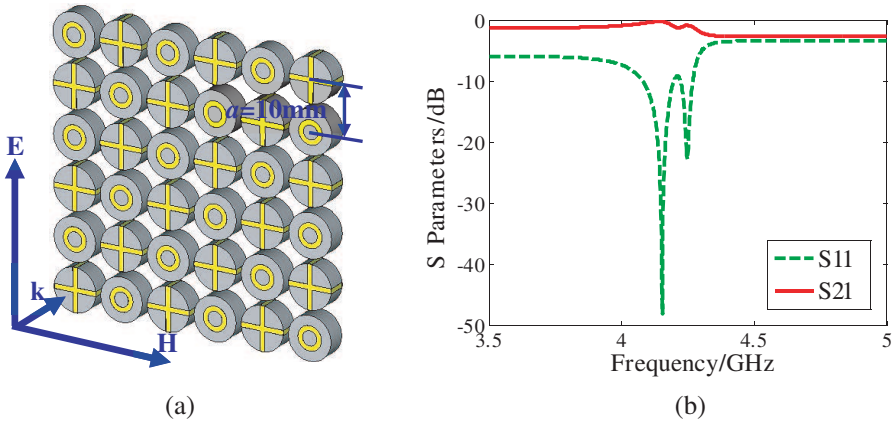

Figure 9. The proposed planar LHM and its transmission spectrum. (a) A layer of the proposed LHM combining the negative-permeability and negative-permittivity unit cells; (b) the transmission spectrum of the planar LHM in Figure 9(a) under normally incident plane waves.

4.55 GHz while the real part of effective permittivity is negative in 4.19 $\sim$ 4.28 GHz. Compared with Figure 5(b) and Figure 8(b), both the negative permeability and negative permittivity ranges shift upwards slightly. This can be explained by the interactions between the negative-permeability and negative-permittivity unit cells. In the frequency range where real parts of both the effective permeability and permittivity are negative, a left-handed band is expected. Figure 10(d)

shows that in the frequency range $4.19 \sim 4.28\,\mathrm{GHz}$, the real part of effective refraction index is negative. The frequency range $4.19 \sim 4.28\,\mathrm{GHz}$ is just the left-handed band we are trying to obtain.

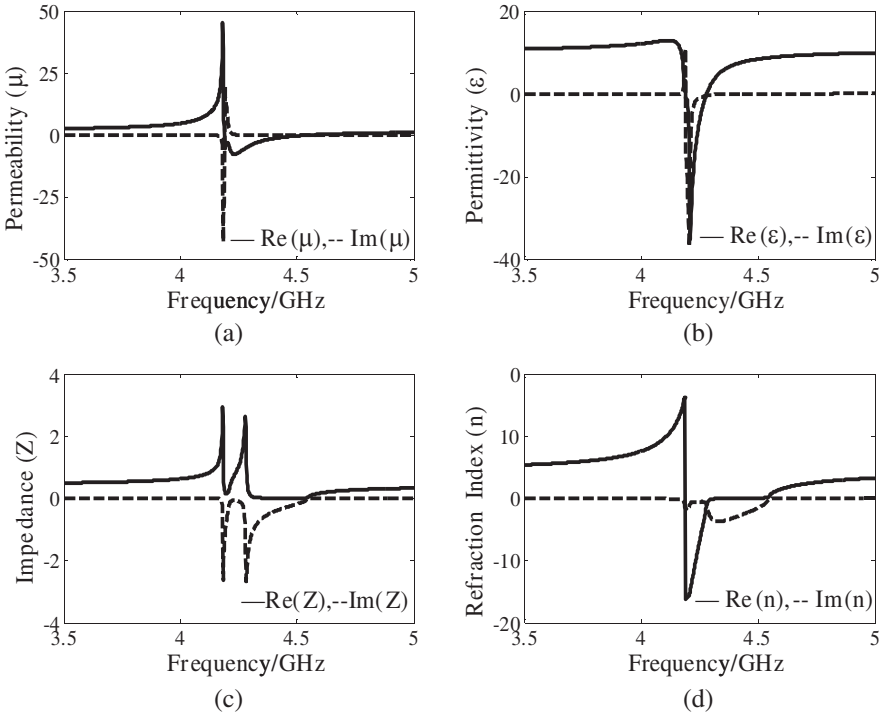

Figure 10. Retrieved constitutive parameters from simulated scattering parameters. (a) Retrieved effective permeability; (b) retrieved effective permittivity; (c) retrieved relative impedance; (d) retrieved refraction index.

3. POLARIZATION-INDEPENDENCE AND WIDE RANGE OF INCIDENCE ANGLES

In Section 2, we just considered the DR-based LHM under normal incidence with a particular polarization. In this section, left-handed properties of the disk-like DR-based LHM under different polarizations and different incidence angles were considered. Incident plane waves with wave vector $\mathbf{k}$ can be characterized by two angles: the incidence angle $\theta \in (0, \pi/2)$ between $\mathbf{k}$ and the surface normal $\mathbf{n}$ of the sample (z direction), and the polarization angle $\varphi \in (-\pi, \pi)$ between the

projection of **k** onto the surface plane and the metallic cross bar along x direction of the unit cell, as shown in Figure 11.

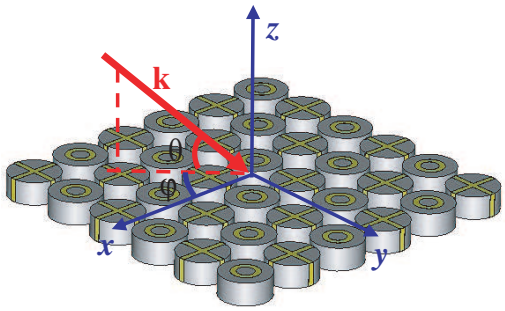

Figure 11. Incidence angle and polarization angle of incidence plane waves with wave vector **k**.

There are two kinds of plane waves: TE and TM plane waves. For normal incident plane waves, the two cases with TE and TM plane waves are the same while for oblique incidences, the two cases are different. When the incident plane waves are TE waves, the electric vector **E** is in parallel with the sample and hence the incidence angle θ is actually the angle between the magnetic vector **H** and surface normal **n** of the sample (z direction). When the incident plane waves are TM waves, the magnetic vector **H** is in parallel with the sample and hence the incidence angle θ is actually the angle between the electric vector **E** and surface normal **n** of the sample (z direction). Thus, we have to consider two cases under oblique incidences, that is, the case with obliquely incident TE plane waves and the case with obliquely incident TM plane waves.

3.1. Left-handed Properties under Different Polarization Angles

Left-handed properties of the disk-like DR-based LHM were investigated under normal incidence with different polarization angles. Under normal incidences, there is no need to consider respectively the TE and TM case.

Figures 12(a), (b) and (c) show, respectively, the retrieved real parts of effective permeability, permittivity and refraction index for the one-unit-cell thick planar LHM in Figure 9(a) under different polarization angles φ and normal incidence. Because of the four-fold rotational symmetry of the negative-permittivity unit cell, it is sufficient to consider $\varphi \in (0, \pi/4)$ for different polarizations. As φ

varies from 0 to $\pi/4$, both the effective permeability and permittivity stay nearly the same. Both the strengths of magnetic and electric resonances become slightly smaller with the polarization angle, but the changes are so minor that they can be neglected. As can be shown in Figures 12(a) and (b), the negative-permeability and negative-permittivity ranges keep unchanged under different polarization angles. Hence, the negative refraction index ranges keeps the same under different polarization angles, as shown in Figure 12(c). Left-handed properties of the planar LHM in Figure 9(a) are polarization-independent.

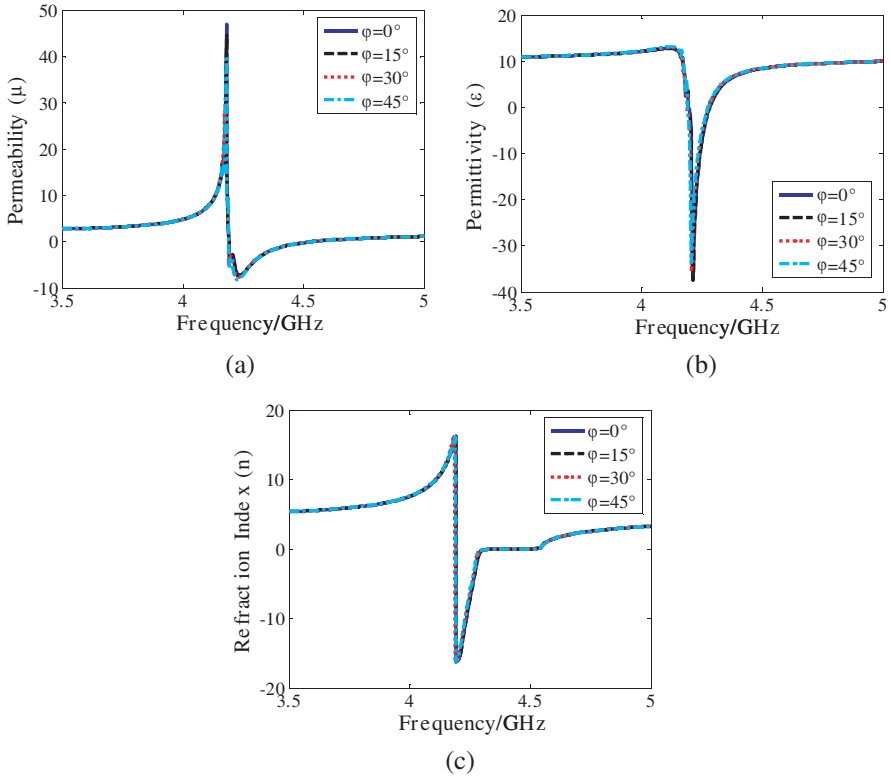

Figure 12. Retrieved real parts of constitutive parameters under different polarization angles $\varphi = 0°$, 15°, 30° and 45°. (a) Real parts of effective permeability; (b) real parts of effective permittivity; (c) real parts of effective refraction index.

3.2. Left-handed Properties under Oblique Incidence TE Plane Waves

For oblique incidence TE plane waves, the electric vector is in parallel with the planar LHM while the angle between the magnetic vector and the LHM surface is the incident angle. In this part, left-handed properties of the planar LHM under obliquely incident TE plane waves with different incident angles were investigated.

Figures 13(a), (b) and (c) show, respectively, the retrieved real parts of effective permeability, permittivity and refraction index for the planar LHM in Figure 9(a) under different oblique incidence TE plane waves with incidence angles $\theta = 0°$, $15°$, $30°$, $45°$ and $60°$. As shown

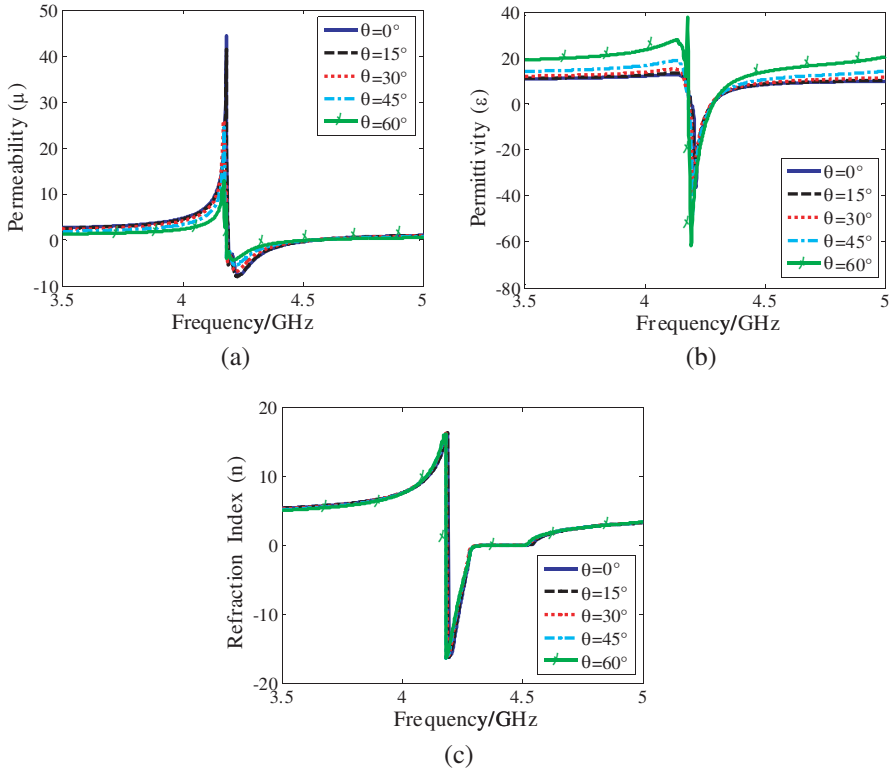

Figure 13. Retrieved real parts of constitutive parameters under different obliquely incident TE plane waves with incidence angles $\theta = 0°$, $15°$, $30°$, $45°$ and $60°$. (a) Real parts of effective permeability; (b) real parts of effective permittivity; (c) real parts of effective refraction index.

in Figures 13(a) and (b), the magnetic resonance becomes a bit weaker while the electric resonance becomes a bit stronger as the incidence angle increases. Since the effective refraction index is the square root of the product of the effective permeability and permeability, the negative index range keeps almost the same under different incidence angles, as shown in Figure 13(c). Moreover, for there is a minor red-shift of the negative-permeability range with the incidence angle, the negative-index range shifts slightly downwards as the incidence angles increases. But the shift is so minor that it can be neglected, so it is reasonable to conclude that left-handed properties of the DR-based planar LHM are approximately the same in the wide incidence angle range $0 < \theta < 60$ under obliquely incident TE plane waves.

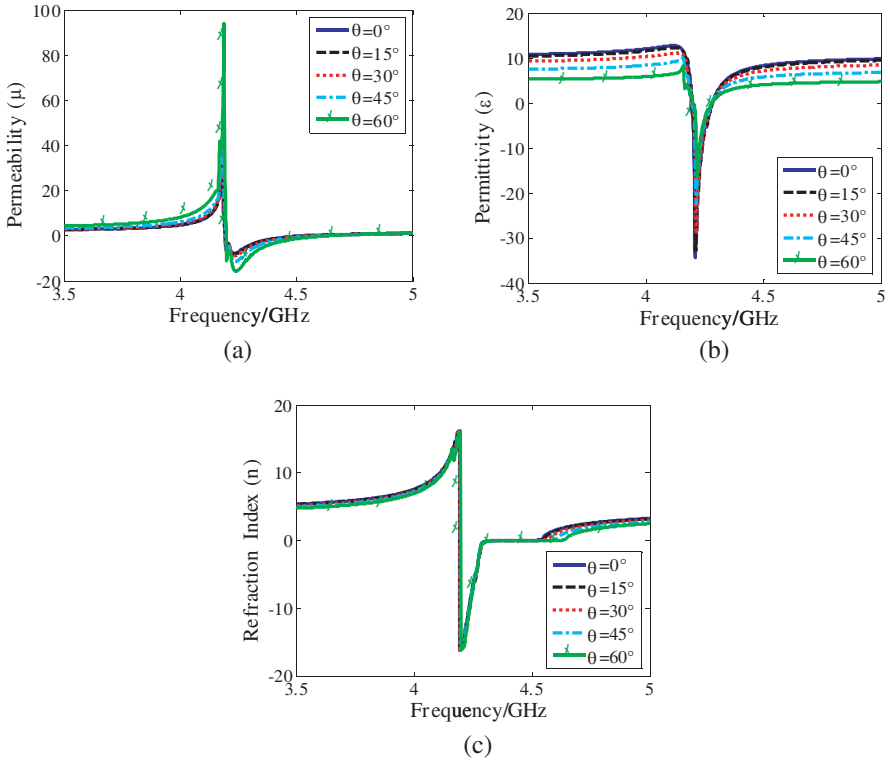

Figure 14. Retrieved real parts of constitutive parameters under different obliquely incident TM plane waves with incidence angles $\theta = 0°$, 15°, 30°, 45° and 60°. (a) Real parts of effective permeability; (b) real parts of effective permittivity; (c) real parts of effective refraction index.

3.3. Left-handed Properties under Oblique Incidence TM Plane Waves

For oblique incidence TM plane waves, the magnetic vector is in parallel with the planar LHM while the angle between the electric vector and the LHM surface is the incident angle. In this part, left-handed properties of the planar LHM under obliquely incident TM plane waves with different incident angles were investigated.

Figures 14(a), (b) and (c) show, respectively, the retrieved real parts of effective permeability, permittivity and refraction index for the planar LHM in Figure 9(a) under different oblique incidence TM plane waves with incidence angles $\theta = 0°$, $15°$, $30°$, $45°$ and $60°$. As shown in Figures 14(a) and (b), the magnetic resonance becomes stronger while the electric resonance becomes weaker as the incidence angle increases. The effective refraction index is the square root of the product of the effective permeability and permeability, so the negative index range keeps almost the same under different incidence angles, as shown in Figure 14(c). Moreover, as shown in Figures 14(a) and (b), there is a minor blue-shift of the negative-permeability range with the incidence angle, so the negative-index range shifts slightly upwards as the incidence angles increases, as shown in Figure 14(c). But the shift is also so minor that it can be neglected, so it is reasonable to conclude that left-handed properties of the DR-based planar LHM are approximately the same in the wide incidence angle range $0 < \theta < 60$ under obliquely incident TM plane waves.

From the above analyses, we can conclude that the disk-like DR-based LHM in Figure 9(a) is independent of polarizations of incident waves and it keeps almost the same left-handed properties in a wide incidence angle range $0< \theta < 60$.

4. CONCLUSIONS

In this paper, a new route for realizing LHMs was presented. It is based on the use of dielectric resonators. Dielectric resonators can be used to realize negative permeability and/or permittivity by etching metallic strips on their surface. As a typical example, we proposed a planar LHM based on disk-like dielectric resonators. By etching metallic strips along the electric fields orientations under $TE_{01\delta}$ and $HEM_{11\delta}$ modes, negative permeability and permittivity are realized, respectively. The proposed planar LHM is independent of polarizations of incident waves. Its left-handed properties keep the same under a wide incident angle range. Since many kinds of dielectric resonator with low loss and good temperature stability are available for practical uses and moreover there are many resonance modes for a particular

kind of dielectric resonator, a great many LHMs can be designed based on dielectric resonators.

ACKNOWLEDGMENT

This work was supported by the National Natural Science Foundation of China (Grant Nos. 50632030 and 60871027).

REFERENCES

1. Pendry, J. B., A. J. Holden, D. J. Robbins, and W. J. Stewart, "Magnetism from conductors and enhanced nonlinear phenomena," *IEEE Trans. Microw. Theory Tech.*, Vol. 47, 2075–2084, 1999.
2. Smith, D. R., W. J. Padilla, D. C. Vier, S. C. Nemat-Nasser, and S. Schultz, "Composite medium with simultaneously negative permeability and permittivity," *Phys. Rev. Lett.*, Vol. 84, 4184–4187, 2000.
3. Xi, S., H. Chen, B.-I. Wu, and J. A. Kong, "Experimental confirmation of guidance properties using planar anisotropic left-handed metamaterial slabs based on S-ring resonators," *Progress In Electromagnetics Research*, PIER 84, 279–287, 2008.
4. Ran, L., J. Huangfu, H. Chen, X. Zhang, K. Cheng, T. M. Grzegorczyk, and J. A. Kong, "Experimental study on several left-handed metamaterials," *Progress in Electromagnetics Research*, PIER 51, 249–279, 2005.
5. Wang, J. F., S. B. Qu, Z. Xu, J. Q. Zhang, Y. M. Yang, H. Ma, and C. Gu, "A candidate three-dimensional GHz left-handed metamaterial composed of coplanar magnetic and electric resonators," *Photon Nanostruct.: Fundam Appl.*, Vol. 6, 183, 2008.
6. Zhou, J. F., L. Zhang, G. Tuttle, T. Koschny, and C. M. Soukoulis, "Negative index materials using simple short wire pairs," *Phys. Rev. B*, Vol. 73, 041101, 2006.
7. Dolling, G., C. Enkrich, M. Wegener, J. F. Zhou, C. M. Soukoulis, and S. Linden, "Cut-wire pairs and plate pairs as magnetic atoms for optical metamaterials," *Opt. Lett.*, Vol. 30, 3198–3200, 2005.
8. Alici, K. B. and E. Ozbay, "A planar metamaterial: Polarization independent fishnet structure," *Photonics Nanostruct.: Fundam. Appl*, Vol. 6, 102–107, 2008.
9. Kafesaki, M., I. Tsiapa, N. Katsarakis, T. Koschny, C. M. Soukoulis, and E. N. Economou, "Left-handed metamaterials: the fish-

net structure and its variations," *Phys. Rev. B*, Vol. 75, 235114, 2007.

10. Guven, K., A. O. Cakmak, M. D. Caliskan, T. F. Gundogdu, M. Kafesaki, C. M. Soukoulis, and E. Ozbay, "Bilayer metamaterial: Analysis of left-handed transmission and retrieval of effective medium parameters," *J. Opt. A: Pure Appl. Opt.*, Vol. 9, 361–365, 2007.
11. Zhou, J. F., T. Koschny, L. Zhang, G. Tuttle, and C. M. Soukoulis, "Experimental demonstration of negative index of refraction," *Appl. Phys. Lett.*, Vol. 88, 221103, 2006.
12. Wang, J. F., S. B. Qu, Z. X, J. Q. Zhang, H. Ma, Y. M. Yang, and C. Gu, "Broadband planar left-handed metamaterials using split-ring resonator pairs," *Photon Nanostruct.: Fundam Appl.*, Vol. 7, 2009 (accepted).
13. Holloway, C. L., E. F. Kuester, J. Baker-Jarvis, and P. Kabos, "A double negative (DNG) composite medium composed of magnetodielectric spherical particles embedded in a matrix," *IEEE Trans. Antennas Propgat.* Vol. 51, No. 10, 2596–2603, 2003.
14. Kim, J. and A. Gopinath, "Simulation of a metamaterial containing cubic high dielectric resonators," *Phys. Rev. B*, Vol. 76, 115126, 2007.
15. Ahmadi, A. and H. Mosallaei, "Physical configuration and performance modeling of all-dielectric metamaterials," *Phys. Rev. B*, Vol. 77, 045104, 2008.
16. Popa, B.-I. and S. A. Cummer, "Compact dielectric particles as a building block for low-loss magnetic metamaterials," *Phys. Rev. Lett.*, Vol. 100, 207401, 2008.
17. Peng, L., L. X. Ran, H. S. Chen, H. F. Zhang, J. A. Kong, and T. M. Grzegorczyk, "Experimental observation of left-handed behavior in an array of standard dielectric resonators," *Phys. Rev. Lett.*, Vol. 98, 157403, 2007.
18. Lepetit, T. and E. Akmansoy, "Magnetism in high-contrast dielectric photonic crystals," *Microwave Opt. Tech. Lett.*, Vol. 50, 909–911, 2008.
19. Jylhä, L., I. Kolmakov, S. Maslovski, and S. Tretyakova, "Modeling of isotropic backward-wave materials composed of resonant spheres," *J. Appl. Phys.*, Vol. 99, 043102, 2006.
20. Kajfez, D. and P. Guillon, Noble Publishing Corp., Georgia, 1998.
21. Chen, X. D., T. M. Grzegorczyk, B.-I. Wu, J. Pacheco, Jr., and J. A. Kong, "Robust method to retrieve the constitutive effective parameters of metamaterials," *Phys. Rev. E*, Vol. 70, 016608,

2004.

22. Smith, D. R., D. C. Vier, T. Koschny, and C. M. Soukoulis, "Electromagnetic parameter retrieval from inhomogeneous metamaterials," *Phys. Rev. E*, Vol. 71, 036617, 2005.
23. Koschny, T., P. Markos, D. R. Smith, and C. M. Soukoulis, "Resonant and antiresonant frequency dependence of the effective parameters of metamaterials," *Phys. Rev. E*, Vol. 68, 065602, 2003.